

Mean opacities of a strongly magnetized high temperature plasma

Valery F. Suleimanov,^{1*} Alexander A. Mushtukov,^{2,3} Igor Ognev,⁴

Victor A. Doroshenko,¹ Klaus Werner¹

¹*Institut für Astronomie und Astrophysik, Kepler Center for Astro and Particle Physics, Universität Tübingen, Sand 1, 72076 Tübingen, Germany*

²*Astrophysics, Department of Physics, University of Oxford, Denys Wilkinson Building, Keble Road, Oxford OX1 3RH, UK*

³*Leiden Observatory, Leiden University, NL-2300RA Leiden, The Netherlands*

⁴*P. G. Demidov Yaroslavl State University, Sovetskaya 14, 150003 Yaroslavl, Russia*

19 October 2022

ABSTRACT

Geometry and dynamical structure of emission regions in accreting pulsars are shaped by the interplay between gravity, radiation, and strong magnetic field, which significantly affects the opacities of a plasma and radiative pressure under such extreme conditions. Quantitative consideration of magnetic plasma opacities is, therefore, an essential ingredient of any self-consistent modeling of emission region structure of X-ray pulsars. We present results of computations of the Rosseland and Planck mean opacities of a strongly magnetized plasma with a simple chemical composition, namely the solar hydrogen/helium mix. We consider all relevant specific opacities of the magnetized plasma including vacuum polarization effect and contribution of electron-positron pairs where the pair number density is computed in the thermodynamic equilibrium approximation. The magnetic Planck mean opacity determines the radiative cooling of an optically thin strongly magnetized plasma. It is by factor of three smaller than non-magnetic Planck opacity at $k_B T < 0.1 E_{\text{cyc}}$ and increases by a factor of $10^2 - 10^4$ at $k_B T > 0.3 E_{\text{cyc}}$ due to cyclotron thermal processes. We propose a simple approximate expression which has sufficient accuracy for the magnetic Planck opacity description. We provide the Rosseland opacity in a tabular form computed in the temperature range 1 – 300 keV, magnetic field range $3 \times 10^{10} - 10^{15}$ G, and a broad range of plasma densities. We demonstrate that the scattering on the electron-positron pairs increases the Rosseland opacity drastically at temperatures > 50 keV in the case of mass densities typical for accretion channel in X-ray pulsars.

Key words: opacity – radiation mechanisms: thermal – polarization – X-rays: binaries – stars: neutron – stars: magnetic field

1 INTRODUCTION

Emission regions of X-ray pulsars (XRP, see e.g., White et al. 1983; Mushtukov & Tsygankov 2022) and pulsing ultraluminous X-ray sources (pULXs) confine high temperature and high density plasma threaded by ultra-strong magnetic fields (Bachetti et al. 2014; Kaaret et al. 2017; Fabrika et al. 2021). Despite many attempts over the last few decades, there are no self-consistent physical models accurately describing the dynamical structure of the emission regions in these objects and their observed X-ray spectra. Two main directions of research can be identified here, i.e. attempts aiming to describe observed spectra based on some simplified assumptions regarding emission region geometry and dynamical structure, and modeling aimed to justify such assumptions from first principles. As an example of first approach one can quote models by Becker & Wolff (2007) Farinelli et al. (2016) which were successfully used for description of the observed spectra of highly-luminous XRP (see e.g. Wolff et al. 2016; Caiazzo &

Heyl 2021), albeit using a rather extended set of free parameters and at times ignoring features like the energy conservation law (Thalhammer et al. 2021). A similar approach was used to model spectra of low-luminous objects (Mushtukov et al. 2021; Sokolova-Lapa et al. 2021), which were recently found to exhibit two-humped X-ray spectra (Tsygankov et al. 2019a,b).

On the other hand, several attempts have been made to model actual physical conditions in the accreting regions, especially in accretion columns. For instance, the pioneering work by Basko & Sunyaev (1976) and many other related investigations (see e.g. Wang & Frank 1981; Lyubarskii & Sunyaev 1988), including two- and three-dimensional modeling of the accretion columns (Postnov et al. 2015; Takahashi & Ohsuga 2017; Gornostaev 2021). Note that understanding of physical conditions in the emitting region of XRP is essential to constrain the maximal possible luminosity of accretion columns, which is relevant for understanding the phenomenon of pULXs (Mushtukov et al. 2015b; Brice et al. 2021). In a first order approximation, the maximal luminosity depends on the optical depth across the column (see e.g. Lyubarskii

* E-mail: suleimanov@astro.uni-tuebingen.de (VFS)

& Syunyaev 1988) and, therefore, on the plasma opacities which remain a major source of uncertainty in such modeling. Indeed, up to now only electron scattering with and without magnetic field were taken into account. In particular, the reduction of the electron scattering cross-section in strong magnetic fields was used by Mushtukov et al. (2015b) to explain the observed high luminosities of pULXs (see also Brice et al. 2021).

Other processes can, however, contribute to the high temperature opacity of plasma in a strong magnetic field. The simplest one is magnetic bremsstrahlung (see e.g. Kaminker et al. 1983). At high plasma temperatures creation of electron-positron pairs due to photon-photon interactions comes into play (see e.g. Beloborodov 1999, and references therein). In presence of strong magnetic fields, also one-photon pair creation becomes relevant (see e.g. Daugherty & Harding 1983). Note that the number density of pairs can be significant in an optically thick plasma in thermodynamic equilibrium especially under the conditions of extremely strong magnetic fields (see e.g. Mushtukov et al. 2019). The increase of pair number density naturally leads to the increase of the opacity. One of the aims of the current work is to compute the Rosseland mean opacity of a high temperature plasma in a strong magnetic field including all the mentioned processes and answer the question whether the aforementioned effects could be relevant for different types of accretion column models.

Here we provide simple means for calculation of the opacity of magnetized plasma and thus make a step towards the accurate calculations of thermal balance in radiative transfer models accounting for a strong external magnetic field, which was an issue for some of the previous investigations. For instance, Sokolova-Lapa et al. (2021) only considered non-magnetized hydrogen plasma emissivity due to bremsstrahlung to compute temperature structures of the overheated upper layers of strongly magnetized neutron star atmospheres heated by accreting protons. We note, however, that plasma cooling and thermal balance could be different if additional cyclotron emission and magnetic bremsstrahlung would be taken into account. The optically thin plasma cooling can be expressed in terms of the Planck mean opacity. Its accurate computation for a high temperature magnetized plasma is the second aim of the paper.

2 METHOD

To calculate the mean Planck $k(\rho, T, B)$ and Rosseland $\kappa(\rho, T, B)$ opacities of a strongly magnetized plasma at given plasma density ρ , temperature T , and magnetic field strength B , we have to determine the plasma chemical composition, number densities of the plasma particles, and cross-sections of the elementary processes of photon interactions with the plasma particles, other photons, and magnetic field. Here we assume that the plasma is the solar hydrogen/helium mix without heavy elements. We assume also that both chemical elements are fully ionized at the considered temperatures $k_B T > 1$ keV, where k_B is the Boltzmann constant.

For computations of the number densities of the plasma particles we have to take into account that the Planck and Rosseland mean opacities are relevant at significantly different physical conditions. The Planck mean opacity de-

scribes the radiation loss rate of an optically thin plasma, $Q = k(\rho, T, B)B(T)$, where $B(T) = \sigma_{\text{SB}}T^4/\pi$ is the integral Planck function, and σ_{SB} is the Stefan-Boltzmann constant. Conversely, the Rosseland mean opacity controls the radiation energy transport in optically thick plasma. Therefore, we assume that the plasma is optically thick and in thermodynamic equilibrium when we compute the Rosseland opacity. In particular it means that the radiation intensity equals the Planck function at the considered temperature. We also assume that the electron-positron pairs are in thermodynamic equilibrium and their number densities can be computed here using this approximation. On the other hand, we cannot exclude physical conditions when the radiation field is still in equilibrium but the pair creation and annihilation is not. Furthermore, the Rosseland mean opacity can be useful for estimates of radiative acceleration in the upper layers of neutron stars (see, e.g. Mushtukov et al. 2015a), i.e. under the assumption of a significantly diluted radiation field. Therefore, we computed three sets of the Rosseland mean opacities for several assumptions regarding the pairs. First, we consider the case with pairs in thermodynamical equilibrium. For the second case pair number density is assumed to be insignificant, but they can be created by photons assuming that the radiation field is described by the Planck function at the considered temperature. Finally, we consider also the case where all processes involving the pairs are ignored.

Pairs certainly cannot be in thermodynamic equilibrium in an optically thin plasma, and we ignore pairs and all the processes connected with pair creations when we compute the Planck opacity. Details of number densities calculations are presented in Appendix A.

We consider all relevant opacity sources in the high-temperature magnetized plasma to compute the Rosseland and Planck means. In particular, we consider specific opacities due to electron scattering κ_{es}^j and free-free absorption κ_{ff}^j (continuum), as well as opacities in the cyclotron resonance and harmonics κ_{cyc}^j . Finally, we treat the processes of electron-positron pair creations by photons as an opacity. We compute the continuum and cyclotron opacities separately in two normal modes, the extraordinary one, X ($j = 1$) and the ordinary one, O ($j = 2$). The opacities due to the two-photon $\kappa_{\gamma\gamma}$ and one-photon pair creation in a strong magnetic field $\kappa_{1\gamma}$ are computed without distinguishing the modes, and we just take them to be equal for both modes. We emphasize that this recipe can also be considered an assumption of our model.

We use approximate expressions rather than precise treatment to simplify the calculations whenever possible. All specific opacities used in the calculations are described in Appendix B. The main approximations used are described here. First, we use the rarified plasma approximation, which means that the plasma frequency $\nu_p = \sqrt{e^2 n_e / \pi m_e}$ is significantly less than the photon frequency ν , and we use the cold plasma approximation for the opacities below the electron cyclotron frequency $\nu_B = eB / 2\pi m_e c$. The corresponding plasma energy is $E_p \approx 0.12 \sqrt{n_e / 10^{25}} \text{ keV}$, and the corresponding non-relativistic cyclotron energy is $E_{\text{cyc}} = \hbar e B / m_e c \approx 11.6 B_{12} \text{ keV}$. Here and further on we use the definition $B_{12} = B / 10^{12} \text{ G}$, and, also, n_e instead of the sum of the electron and positron number densities, $n_e = n_{e^-} + n_{e^+}^B$ when the Rosseland mean opacities are considered.

The specific total opacity $\kappa^j(E, \mu)$ at the photon energy

E depends on $\mu = \cos \theta$, where θ is the angle between the photon momentum and the magnetic field direction, and is computed as

$$\kappa^j(\mu, E) = \kappa^j(\mu, E) + \max(\kappa_{\text{es}}^j, (1 - \mathcal{P})\kappa_{\text{cyc}}^j) + \kappa_{\gamma\gamma} + \kappa_{1\gamma}. \quad (1)$$

The first term is the true opacity

$$\kappa^j(\mu, E) = \max(\kappa_{\text{ff}}^j, \mathcal{P}\kappa_{\text{cyc}}^j), \quad (2)$$

which includes free-free absorption and thermal cyclotron emission. Here we took into account the fact, that the continuum opacities and the cyclotron opacity are closely tied and have to be considered and computed simultaneously. However, we describe both here as different processes in the framework of the adopted approximations. Therefore, we compare κ_{es}^j with $(1 - \mathcal{P})\kappa_{\text{cyc}}^j$ and κ_{ff}^j with $\mathcal{P}\kappa_{\text{cyc}}^j$ at every photon energy, and only take into account the largest opacity.

The main processes of excitation and de-excitation of upper Landau levels are interactions with photons. On the other hand, de-excitation and excitation by thermal ions also contribute to the total rate of excitation and de-excitation. Thus, the process where excitation is due to photon and de-excitation is due to collision with an ion must be considered as a true opacity. The opposite process provides additional plasma cooling. The relative contribution of the thermal processes to the total cyclotron opacity \mathcal{P} can be expressed as it was described by Pavlov et al. (1980b), see also discussion in Potekhin (2014)

$$\mathcal{P} = \frac{\nu_{\text{ei}}}{\nu_{\text{ei}} + \nu_{\text{er}}} \approx \frac{\nu_{\text{ei}}}{\nu_{\text{er}}}, \quad (3)$$

where ν_{er} is the frequency of the electron-photon collisions and ν_{ei} is the frequency of the electron-ion collisions. We used, however, the full \mathcal{P} definition (the left side of Eq. 3) in the computations.

The collision frequencies are determined as (see e.g. van Adelsberg & Lai 2006)

$$\nu_{\text{er}} \approx \frac{2e^2}{3\hbar^2 m_e c^3} E^2 \approx 1.446 \times 10^{13} E_{\text{keV}}^2 \quad (4)$$

$$\begin{aligned} \nu_{\text{ei}} &\approx \frac{4\pi}{3\sqrt{3}} \bar{Z}^2 e^4 \left(\frac{2\pi}{m_e kT} \right)^{1/2} \frac{n_{\text{ion}}}{E} \left[1 - \exp\left(-\frac{E}{k_B T}\right) \right] \\ &\approx 1.93 \times 10^{-10} \frac{n_{\text{ion}}}{T_{\text{keV}}^{1/2} E} \left[1 - \exp\left(-\frac{E}{k_B T}\right) \right]. \end{aligned} \quad (5)$$

Therefore,

$$\mathcal{P} \approx 1.3 \times 10^{-23} \frac{n_{\text{ion}}}{T_{\text{keV}}^{1/2} E^3} \left[1 - \exp\left(-\frac{E}{k_B T}\right) \right]. \quad (6)$$

This value agrees to an order of magnitude with the estimation made by Arons et al. (1987), i.e. given by their Eqs. (64) and (66). It is also similar to the value presented by Mushtukov et al. (2021), i.e. given by their Eq. (19), if we assume that $E = k_B T = E_{\text{cyc}}$. The estimates in both papers cited above were made, however, for the cyclotron line only, so our result is acceptable in a wider energy range.

It is also important to realize that mean opacities of a magnetized plasma depend on the angle between the magnetic field lines and the direction of the photon propagation. We computed the Rosseland mean for two such angles, across and along magnetic field for both polarization normal modes.

The Rosseland mean across the field is computed as it was described by Mushtukov et al. (2015b)

$$\kappa_{\perp}^j = \frac{\int_0^\infty dB_E/dT dE}{\int_0^\infty dB_E/dT dE \int_0^\pi d\varphi \int_0^1 3\mu_n^2 [\pi\kappa_j(\mu, E)]^{-1} d\mu_n}, \quad (7)$$

where E is the photon energy, and B_E is the Planck function. The angular integration occurs around the main axis normal to the magnetic field direction, and φ is the azimuthal angle, and μ_n is the cosine of the angle between the photon momentum and the main axis. We note that the specific total opacity $\kappa_j(E, \mu)$ at photon energy E depends on the cosine $\mu = \cos \theta$, where θ is the angle between photon momentum and magnetic field direction. Both cosines are connected as $\mu = \sqrt{1 - \mu_n^2} \cos \varphi$. We note that $\kappa_j(\mu, E)$ depends also on plasma temperature and density.

The Rosseland mean opacity along the magnetic field is computed more easily due to axial symmetry (Mushtukov et al. 2015a)

$$\kappa_{\parallel}^j = \frac{\int_0^\infty dB_E/dT dE}{\int_0^\infty dB_E/dT dE \int_0^1 3\mu^2 [\kappa_j(\mu, E)]^{-1} d\mu}. \quad (8)$$

The Planck mean opacities in the both directions are computed in a similar manner, but here we only considered the opacity along the field, because there is an obvious astrophysical application only for this case (see e.g. Sokolova-Lapa et al. 2021):

$$k_{\parallel}^j = \frac{\pi \int_0^\infty B_E dE \int_0^1 k_j(\mu, E) d\mu}{\sigma_{\text{SB}} T^4}, \quad (9)$$

with the same notation. We note, that the both mean opacities are computed in the plasma rest-frame.

The mean opacities computed separately in two polarization modes were summed using following rules

$$\frac{1}{\kappa_{\perp, \parallel}} = \frac{1}{2\kappa_{\perp, \parallel}^{\text{X}}} + \frac{1}{2\kappa_{\perp, \parallel}^{\text{O}}} \quad \text{and} \quad k_{\parallel} = \frac{k_{\parallel}^{\text{X}}}{2} + \frac{k_{\parallel}^{\text{O}}}{2}. \quad (10)$$

We mix the Rosseland opacities for both modes in equal proportions because electron scattering effectively mixes the polarization modes in the optically thick plasma, where the Rosseland mean opacity has to be used. This is a consequence of the assumption of local thermodynamical equilibrium in the plasma, which is optically thick in both modes. In particular, this assumption $I_E^j = B_E/2$ is used as the inner boundary condition for the radiation transfer equations in the normal modes (Shibanov et al. 1992). Cooling of a plasma optically thin in both modes occurs independently in both modes, $Q^j = k_{\parallel}^j B/2$, and the total cooling rate is reduced to $Q = (k_{\parallel}^{\text{X}}/2 + k_{\parallel}^{\text{O}}/2)B(T)$.

Integration over photon energies cannot be performed from zero to infinity in numerical computations. Therefore, we used finite limits during the computations. It is important to cover a wide band around the Planck function maximum at a given temperature. Therefore, we take the energy band for computing the mean opacities at given temperature between $0.01 k_B T$ and $30 k_B T$. Values of the Planck function at the boundaries are at least by four orders of magnitude lower

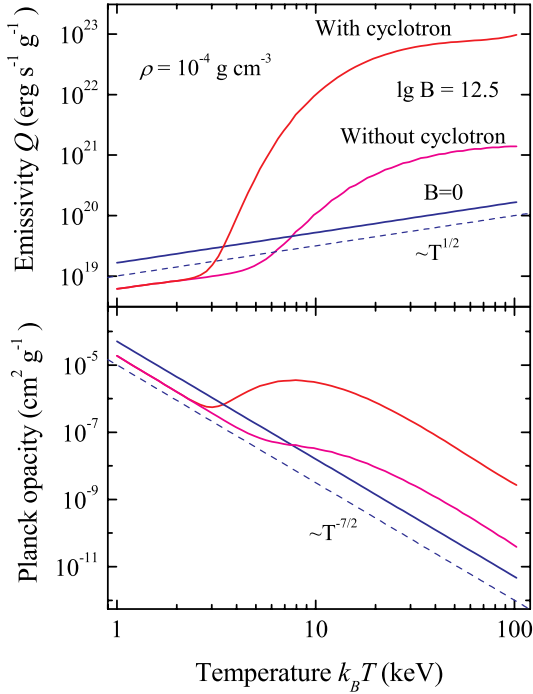


Figure 1. Dependencies of the magnetized plasma emissivity (top panel) and the Planck mean opacity (bottom panel) on the plasma temperature for magnetic field strength $B = 10^{12.5}$ G computed with and without contribution of the cyclotron emission. The corresponding values computed for non-magnetized plasma are also shown. The plasma density is $\rho = 10^{-4}$ g cm⁻³.

compared to the maximum, and this fact guarantees that the outside energy bands do not contribute significantly to the mean opacity.

3 RESULTS

Thermal cyclotron emission significantly contributes to the Planck opacity and, therefore, to radiative energy losses at some temperatures, see Fig. 1. The Planck opacity of the magnetized plasma is lower by about a factor of two to three compared to the corresponding opacity of the non-magnetized plasma if the plasma temperature is much less than the cyclotron energy ($k_B T \leq 0.1 E_{\text{cyc}}$). The main reason is that the opacity in X-mode is depressed and only the O-mode contributes to the opacity under this condition. The cyclotron thermal emission completely dominates at $k_B T > 0.3 E_{\text{cyc}}$ increasing the Planck opacity by approximately three orders of magnitude. We note, however, that the Planck opacity of the magnetized plasma increases even if we ignore thermal cyclotron emission ($\mathcal{P} = 0$), which is due to the contribution of peaks in the Gaunt factor at the cyclotron harmonics (see Pavlov & Panov 1976; Suleimanov et al. 2010; Potekhin 2010).

The dependence of the Planck mean opacity on the magnetic field strength is shown in Fig. 2. It can be seen that the Planck opacity properties are consistent with the description presented above. However, the contribution of thermal

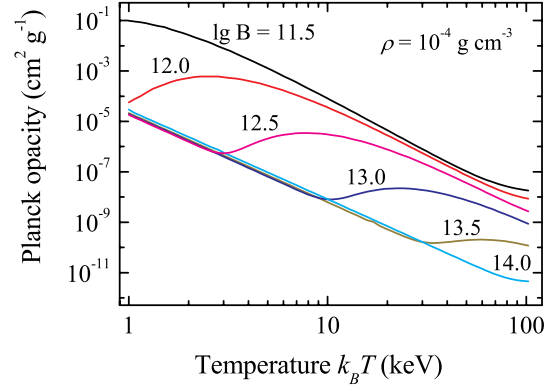


Figure 2. Dependencies of the magnetized plasma Planck mean opacities on the plasma temperature for various magnetic field strengths and plasma density $\rho = 10^{-4}$ g cm⁻³.

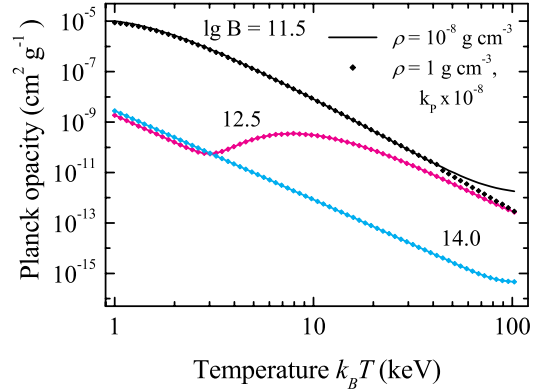


Figure 3. Comparison of the Planck mean opacities computed for two different plasma densities, $\rho = 10^{-8}$ g cm⁻³ and $\rho = 1$ g cm⁻³, and three various magnetic field strengths. The opacities computed for the higher density were multiplied by a factor of 10^{-8} .

cyclotron emission becomes relatively less important as the magnetic field strength increases. It is well known, that the Planck opacity of a non-magnetized plasma depends linearly on plasma density. The same is correct for a magnetized plasma, see Fig. 3, where the normalized Planck opacities computed for $\rho = 10^{-8}$ g cm⁻³ and $\rho = 1$ g cm⁻³, and three various magnetic field strengths are shown. Note that there is some inconsistency at the lowest magnetic field and the highest temperature, which is related to the fact that the approximations used for the cyclotron opacity at these plasma parameters start to fail here because the cyclotron harmonics strongly overlap at these conditions, and much more complicated computations are necessary (see e.g. Chanmugam & Dulk 1981). For that reason we did not consider here the Planck opacity of a relatively low magnetized plasma with $B < 10^{11}$ G.

We also find a relatively simple analytic function which can be used to approximate the numerical computations of

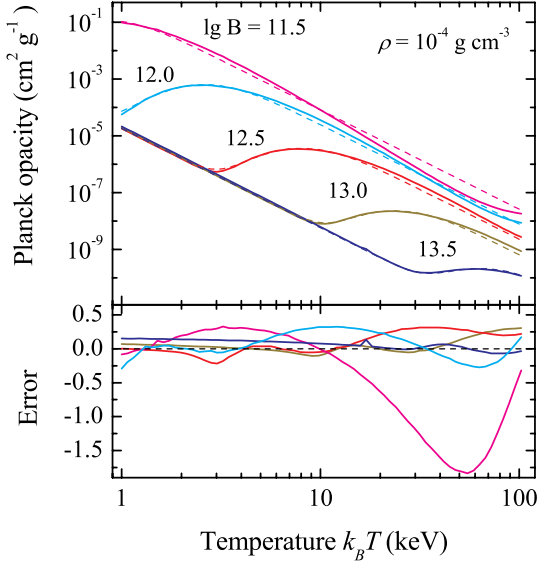


Figure 4. *Top panel:* Results of the approximation of the dependencies of the Planck mean opacities on the plasma temperature for various magnetic field strengths (solid curves)

with the approximation formula (11, dashed curves). The plasma density is $\rho = 10^{-4} \text{ g cm}^{-3}$. *Bottom panel:* Relative errors of the fitting.

the Planck mean opacities:

$$\tilde{k}_{\parallel} = 0.36 k_0 \left(1 + A_{\text{cyc}} \left(1 - \exp \left[-\frac{k_B T}{0.1 E'_{\text{cyc}}} \right] \right)^{13.4} \right), \quad (11)$$

where k_0 is the Planck mean, computed for the non-magnetized plasma at given density and temperature

$$k_0 = 0.5058 \rho T_{\text{keV}}^{-3.5}, \quad (12)$$

and the cyclotron energy E' computed across the field using the relativistic formula

$$E'_{\text{cyc}} = m_e c^2 \left(\sqrt{1 + 2 \frac{B}{B_{\text{cr}}}} - 1 \right). \quad (13)$$

The amplification factor A_{cyc} is also dependent on the magnetic field strength and is

$$A_{\text{cyc}} \approx 4240 B_{12}^{-1.06}. \quad (14)$$

Here $B_{\text{cr}} = 4.414 \times 10^{13} \text{ G}$, see also Appendix A.

Some examples illustrating the parametrization of numerical calculations with this function are shown in Fig. 4. The relative accuracy of the fitting $(k_{\parallel} - \tilde{k}_{\parallel})/k_{\parallel}$ is not high, about 10–30%. The error is larger for low magnetic fields and can reach 200% for the lowest magnetic field at high temperatures. This means that we recommend using the approximation formula (11) with caution for astrophysical problems requiring high accuracy. We note, however, also that the uncertainties due to the simplifications used for numerical calculations, especially for the contribution of thermal cyclotron emission \mathcal{P} could be comparable with the approximation formula uncertainties.

The dependence of the Rosseland mean opacity on plasma density is more complex. Therefore, we computed an extended grid of Rosseland opacities for both, across and along

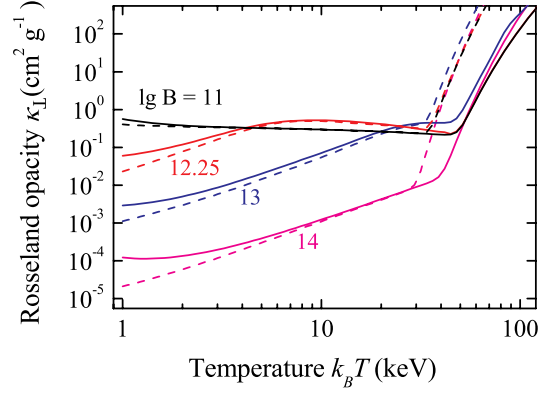


Figure 5. Dependencies of the Rosseland mean opacities across the magnetic field on the plasma temperature for various magnetic field strengths and two plasma density parameters, $\rho = 0.1$ (dashed curves) and 10 g cm^{-3} (solid curves). The magnetic field strengths are marked near the curves.

the field lines for 85 plasma temperatures, from $\lg T_{\text{keV}} = 0$ to 2.52 with the step 0.03, and 14 magnetic field strengths $\lg B = 10.5, 11, 11.5, 11.75, 12, 12.25, 12.5, 12.75, 13, 13.25, 13.5, 14, 14.5$, and 15. The third grid parameter is density. This parameter has 19 values on the grid, from $\lg \rho = -6$ to 3 with the step 0.5. We note that the electrons at the lowest plasma temperatures and magnetic field strength are degenerate. Our approach is not strictly correct for degenerate plasma, and the opacities under such conditions are, therefore, not computed. Instead, the opacity values computed for the lower plasma density are taken. It is important, that the magnetic field is strongly quantizing for the considered plasma parameters at $k_B T < E_{\text{cyc}}$. It means that all the electrons are in the first Landau level and the Fermi temperature is significantly less than the Fermi temperature for the non-quantizing magnetic field (see Appendix A). As a result, electrons are not degenerate even at the lowest temperatures and the highest densities if $\lg B \geq 11.75$.

Examples of the computed Rosseland mean opacities κ_{\perp} from the first set for a few magnetic field strengths and two density values, $\rho = 0.1$ and 10 g cm^{-3} , are shown in Fig. 5. A significant increase of the opacity at $k_B T > 40$ –100 keV is connected with the scattering on the electron-positron pairs. The opacities at lower temperatures are generally consistent with the case of pure magnetic electron scattering presented by Mushtukov et al. (2015b). The opacities of a dense plasma are higher than the opacities of a rarified plasma due to increase of the free-free opacity contribution. The opacities for $B = 10^{11} \text{ G}$ are close to the case of the non-magnetized plasma, and the opacities have a local maximum at temperatures of about 10 keV for a moderate magnetized plasma ($\lg B = 12.25$) due to the contribution of the cyclotron line and its harmonics.

A comparison of the Rosseland opacities κ_{\perp} computed for all three considered cases is shown in Fig. 6. The opacities from the second case increase at temperatures above 100 keV mainly due to photon-photon interactions. We note, that increase of opacity occurs at the higher temperatures (about 60–70 keV instead of 30 keV in the example above), and the

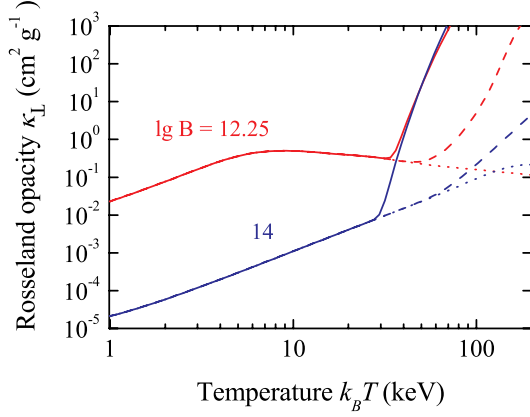


Figure 6. Comparison of the Rosseland κ_{\perp} opacities computed with (solid curves) and without (dashed curves) electron-positron pairs taking into account. The opacities computed without considering pairs are also shown (dotted curves)

The results for two magnetic field strengths, $\lg B = 12.25$ and $\lg B = 14$, and $\rho = 0.1 \text{ g cm}^{-3}$ are shown.

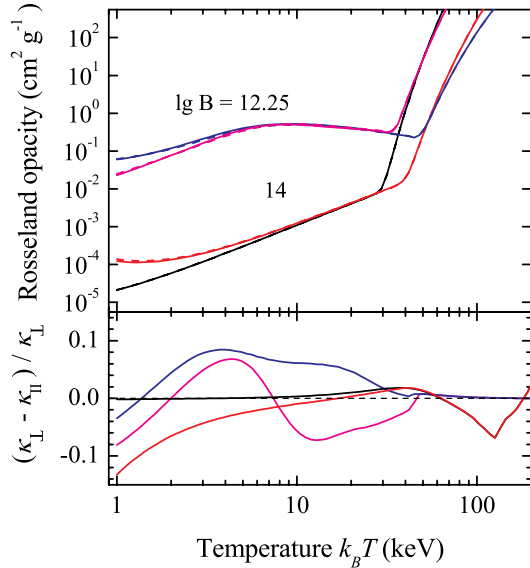


Figure 7. Comparison of the Rosseland mean opacities across (solid curves) and along (dashed curves) the magnetic field for two field strengths and two plasma density parameters, $\rho = 0.1$ and 10 g cm^{-3} . The magnetic field strengths are marked near the curves. The relative differences between opacities are shown in the bottom panel.

opacity is reduced by several orders of magnitude for temperatures above 30 keV. This computations are not completely self-consistent because the photon-photon interactions lead to pair creation. However, these results allow us to qualitatively estimate a value of the Rosseland opacity when the pair number density is far from the equilibrium. Opacities, computed for the third case, show no significant increase at

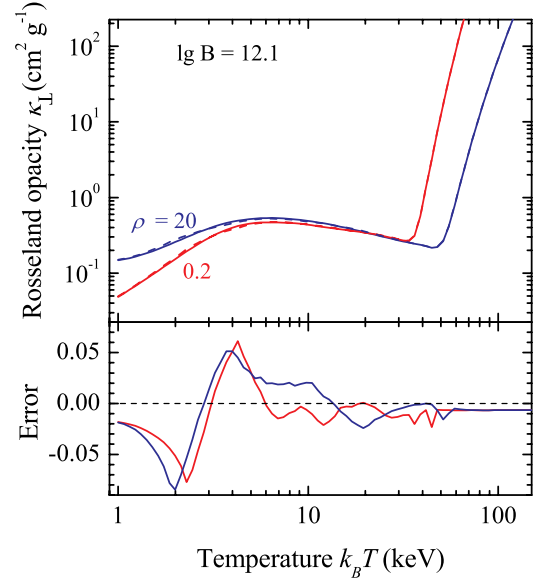


Figure 8. *Top panel:* Comparison of the interpolated opacities (dashed curves) with the exactly computed ones (solid curves) for two plasma density parameters, $\rho = 0.2$ (red curves) and 20 g cm^{-3} (blue curves). The magnetic field strength is fixed ($\lg B = 12.1$). *Bottom panel:* Dependence of the relative interpolation errors ($[\text{exact} - \text{interpolated}] / \text{exact}$) on the plasma temperature.

high temperatures as all the processes connected with pairs are ignored in this set.

A comparison of the Rosseland opacity across and along the field is presented in Fig. 7. In fact, the Rosseland κ_{\perp} and κ_{\parallel} are close to each other with maximum differences of about 10-15%. The opacities from the first set were used here and further.

A code for the interpolation in the grid was also created. the code is based on the spline interpolation procedure MAP1 created by R.L. Kurucz and published in his code ATLAS (Kurucz 1970). Examples of the relative interpolation accuracy for κ_{\perp} ($\text{error} = (\kappa_{\perp}(\text{comp}) - \kappa_{\perp}(\text{interp})) / \kappa_{\perp}(\text{comp})$) are shown in Fig. 8. The interpolation accuracy is better than 10% for all temperatures. We note that we presented the most complicated case when the contribution of the cyclotron opacity is important ($\lg B$ between 11.75 and 12.5). The interpolation accuracy is far better at lower and higher magnetic fields. The source files in the arXiv publication contain the interpolation code together with the necessary data files and a test example.

4 CONCLUSIONS

We investigated the properties of the Rosseland and Planck mean opacities of a high-temperature plasma in a strong magnetic field. Using accurate values of these opacities is important for the construction of accretion structures on the surface of neutron stars in X-ray pulsars, namely accretion columns and accretion heated spots.

We considered a plasma with a simplified chemical composition, the solar hydrogen/helium mix. We also assumed

that both chemical elements are fully ionized at the considered temperature range $k_B T$, 1–330 keV, and that the plasma density is low enough to be non-degenerate. Finally, we also assumed that the plasma temperature is larger than the energy corresponding to the plasma frequency, $k_B T \gg E_p$.

All specific opacities relevant for radiative transfer in a highly magnetized plasma were considered. They included magnetic bremsstrahlung, magnetic electron scattering, cyclotron line and harmonics, and the one- and two-photon pair creations. Magnetic bremsstrahlung and electron scattering were considered in the cold plasma approximations at photon energies $E \leq E_{cyc}$, and various simplifying approximations were used for the description of the cyclotron opacity. All these three opacity sources were computed for two modes of radiative transfer in a highly magnetized plasma.

We demonstrated that the Planck mean opacity of a highly magnetized plasma has the main properties similar to the Planck mean opacity of the fully ionized non-magnetized plasma. In particular, it is also linearly proportional to the plasma density. The Planck opacity of the highly magnetized plasma is by factor of three lower than the corresponding opacity of the non-magnetized plasma at temperatures $k_B T < 0.1 E_{cyc}$, because only the opacity in the ordinary mode is significant, and the additional reduction arises due to magnetic Gaunt factor behaviour. At higher temperatures, the contribution of thermal cyclotron absorption becomes significant and the Planck opacity increases by a few orders of magnitude reaching a maximum at $k_B T \approx 0.3 E_{cyc}$. The opacity amplification is maximum for the lowest magnetic field strength considered ($B \approx 3.3 \times 10^{11}$ G) and decreases almost linearly as the magnetic field strength increases. At the same time, the contribution of the thermal cyclotron emission to plasma cooling is the largest source of uncertainty for plasma cooling rate, because existing computations of the ratio between the thermal cyclotron emission and the cyclotron scattering are not robust.

We suggest a relatively simple approximation formula (11) for the description of the Planck opacity of a high temperature plasma in a strong magnetic field. We demonstrated that this approximation has an accuracy of about 30% for $\lg B \geq 12$ and can be used for modeling of the radiative cooling of the high-magnetized plasma.

The Rosseland mean opacity does not depend on the plasma density linearly, and we computed an extended grid of these opacities both, along and across the field for plasma temperatures from 1 to 330 keV and 14 values of the magnetic field strength in the range $\lg B$ from 10.5 to 15. The third input parameter of the grid is the plasma density ρ ranging between 10^{-6} and 10^3 . The electrons are degenerate at a few of the lowest temperatures and high densities for low magnetic field strength, and the opacities at these grid points were not computed. The electrons at strongly quantizing magnetic field, $\lg B \geq 11.75$ for the adopted grid are not degenerate even at the lowest temperatures and the highest densities. The main difference of our work in comparison with the calculations previously published in the literature is the inclusion of scattering on the electron-positron pairs. Their number densities needed for such calculation were computed by us using thermodynamic equilibrium assumption in the non-relativistic approximation. Formally, the opacities connected with electron-positron pair creation on the two-photon interaction and the photon interaction with a strong mag-

netic field were also included to the Rosseland opacity computations. However, their contribution to the total opacity is insignificant in comparison with the scattering on the pairs. Altogether, we computed three sets of Rosseland mean opacities across and along the field. In the first set we take into account pairs in the thermodynamical equilibrium assumption and opacities due to pair creation in the thermodynamic equilibrium radiation field. In the second set we assumed that there are no pairs, but their creation in the Planck radiation field is possible. In the last set we ignored the pairs completely.

We did not include the pair annihilation as an additional source of the radiative cooling of the magnetized plasma, e.g. in the Planck opacity calculations. This process can be pre-computed assuming that the radiation intensity equals the Planck function, but it is not correct for the optically thin plasma layers where the Planck opacity has to be used.

The inclusion of scattering on the pairs leads to the Rosseland mean opacity dramatically increasing at temperatures $k_B T > 50 - 100$ keV, especially for the strong magnetic field cases. This fact refutes earlier results where it was demonstrated that the maximum accretion column luminosities increase as the magnetic field strength on the neutron star surface increases (Mushtukov et al. 2015b; Brice et al. 2021). New computations of the maximum accretion column luminosities with the Rosseland mean opacities computed here taken into account will be published in a separate paper. Preliminary results are presented by Suleimanov et al. (2022). There it is shown that the maximum luminosity of the accretion column ceases to grow with increasing magnetic field at $\lg B \approx 14.5$, while in the papers cited above the maximum luminosity monotonically grows with increasing magnetic field.

ACKNOWLEDGEMENTS

This work was supported by Deutsche Forschungsgemeinschaft (DFG) (grant WE 1312/53-1). AAM thanks UKRI Stephen Hawking fellowship and the Netherlands Organization for Scientific Research Veni Fellowship.

DATA AVAILABILITY

The Rosseland opacity tables together with the interpolation code will be shared on reasonable request to the corresponding author. They are also available at the arXiv publication and via https://github.com/alexandermushtukov/RT_mag_opacity.

REFERENCES

- Arons J., Klein R. I., Lea S. M., 1987, *ApJ*, **312**, 666
- Asplund M., Grevesse N., Sauval A. J., Scott P., 2009, *ARA&A*, **47**, 481
- Bachetti M., Harrison F. A., Walton D. J., Grefenstette B. W., Chakrabarty D., et al. 2014, *Nature*, **514**, 202
- Baring M. G., 1991, *A&A*, **249**, 581
- Basko M. M., Sunyaev R. A., 1976, *MNRAS*, **175**, 395
- Becker P. A., Wolff M. T., 2007, *ApJ*, **654**, 435
- Beloborodov A. M., 1999, *MNRAS*, **305**, 181
- Brice N., Zane S., Turolla R., Wu K., 2021, *MNRAS*, **504**, 701
- Caiazzo I., Heyl J., 2021, *MNRAS*, **501**, 109

- Chanmugam G., Dulk G. A., 1981, *ApJ*, **244**, 569
- Daugherty J. K., Harding A. K., 1983, *ApJ*, **273**, 761
- Fabrika S. N., Atapin K. E., Vinokurov A. S., Sholukhova O. N., 2021, *Astrophysical Bulletin*, **76**, 6
- Farinelli R., Ferrigno C., Bozzo E., Becker P. A., 2016, *A&A*, **591**, A29
- Ginzburg V. L., 1970, The propagation of electromagnetic waves in plasmas. International Series of Monographs in Electromagnetic Waves, Oxford: Pergamon
- Gornostaev M. I., 2021, *MNRAS*, **501**, 564
- Haensel P., Potekhin A. Y., Yakovlev D. G., 2007, Neutron Stars 1 : Equation of State and Structure. Astrophysics and space science library Vol. 326, New York: Springer
- Kaaret P., Feng H., Roberts T. P., 2017, *ARA&A*, **55**, 303
- Kaminker A. D., Yakovlev D. G., 1993, Soviet Journal of Experimental and Theoretical Physics, **76**, 229
- Kaminker A. D., Pavlov G. G., Shibano I. A., 1983, *Ap&SS*, **91**, 167
- Kurucz R. L., 1970, SAO Special Report, **309**
- Lai D., Ho W. C. G., 2003, *ApJ*, **588**, 962
- Lyubarskii Y. E., Syunyaev R. A., 1988, Soviet Astronomy Letters, **14**, 390
- Melrose D. B., Zhelezniakov V. V., 1981, *A&A*, **95**, 86
- Mushtukov A., Tsygankov S., 2022, arXiv e-prints, p. arXiv:2204.14185
- Mushtukov A. A., Suleimanov V. F., Tsygankov S. S., Poutanen J., 2015a, *MNRAS*, **447**, 1847
- Mushtukov A. A., Suleimanov V. F., Tsygankov S. S., Poutanen J., 2015b, *MNRAS*, **454**, 2539
- Mushtukov A. A., Nagirner D. I., Poutanen J., 2016, *Phys. Rev. D*, **93**, 105003
- Mushtukov A. A., Ognev I. S., Nagirner D. I., 2019, *MNRAS*, **485**, L131
- Mushtukov A. A., Suleimanov V. F., Tsygankov S. S., Portegies Zwart S., 2021, *MNRAS*, **503**, 5193
- Paczynski B., 1983, *ApJ*, **267**, 315
- Pandya A., Zhang Z., Chandra M., Gammie C. F., 2016, *ApJ*, **822**, 34
- Pavlov G. G., Panov A. N., 1976, Soviet Journal of Experimental and Theoretical Physics, **44**, 300
- Pavlov G. G., Shibano I. A., Iakovlev D. G., 1980a, *Ap&SS*, **73**, 33
- Pavlov G. G., Mitrofanov I. G., Shibano I. A., 1980b, *Ap&SS*, **73**, 63
- Postnov K. A., Gornostaev M. I., Klochkov D., Laplace E., Lukin V. V., Shakura N. I., 2015, *MNRAS*, **452**, 1601
- Potekhin A. Y., 2010, *A&A*, **518**, A24
- Potekhin A. Y., 2014, *Physics Uspekhi*, **57**, 735
- Potekhin A. Y., Lai D., Chabrier G., Ho W. C. G., 2004, *ApJ*, **612**, 1034
- Poutanen J., 2017, *ApJ*, **835**, 119
- Schwarm F. W., et al., 2017, *A&A*, **597**, A3
- Shibano I. A., Zavlin V. E., Pavlov G. G., Ventura J., 1992, *A&A*, **266**, 313
- Sokolova-Lapa E., et al., 2021, *A&A*, **651**, A12
- Suleimanov V., Potekhin A. Y., Werner K., 2009, *A&A*, **500**, 891
- Suleimanov V. F., Pavlov G. G., Werner K., 2010, *ApJ*, **714**, 630
- Suleimanov V., Poutanen J., Werner K., 2012a, *A&A*, **545**, A120
- Suleimanov V. F., Pavlov G. G., Werner K., 2012b, *ApJ*, **751**, 15
- Suleimanov V., Mushtukov A., Ognev I., Doroshenko V., Werner K., 2022, arXiv e-prints, p. arXiv:2208.14237
- Takahashi H. R., Ohsuga K., 2017, *ApJ*, **845**, L9
- Thalhammer P., et al., 2021, *A&A*, **656**, A105
- Tsygankov S. S., Rouco Escorial A., Suleimanov V. F., Mushtukov A. A., Doroshenko V., Lutovinov A. A., Wijnand s R., Poutanen J., 2019a, *MNRAS*, **483**, L144
- Tsygankov S. S., Doroshenko V., Mushtukov A. A., Suleimanov V. F., Lutovinov A. A., Poutanen J., 2019b, *MNRAS*, **487**, L30
- Wang Y. M., Frank J., 1981, *A&A*, **93**, 255
- White N. E., Swank J. H., Holt S. S., 1983, *ApJ*, **270**, 711
- Wolff M. T., et al., 2016, *ApJ*, **831**, 194
- Zeldovich Y. B., Novikov I. D., 1971, Relativistic astrophysics. Vol.1: Stars and relativity. University of Chicago Press, Chicago
- van Adelsberg M., Lai D., 2006, *MNRAS*, **373**, 1495

APPENDIX A: ELECTRON AND ION NUMBER DENSITIES

The electron and ion number densities are determined by two equations, the electric neutrality of the plasma

$$n_{e-} = n_{e+}^B + \bar{Z} n_{\text{ion}} \quad (\text{A1})$$

and the relation between the ion number density and the plasma density

$$n_{\text{ion}} = \frac{\rho}{\bar{A} m_H}. \quad (\text{A2})$$

Here n_{e+}^B is the positron number density at the given magnetic field strength, and this value was taken equal to zero at the Planck opacity computations, $\bar{Z} = A_H + 2A_{\text{He}}$ is the average ion charge, and $\bar{A} = A_H + 4A_{\text{He}}$ is the average ion mass. We take the relative hydrogen number density $A_H = 0.922$ and the relative helium number density $A_{\text{He}} = 0.078$ according to Asplund et al. (2009). Therefore, the number densities of hydrogen and helium are computed as follows:

$$n_H = A_H n_{\text{ion}}, \quad n_{\text{He}} = A_{\text{He}} n_{\text{ion}}. \quad (\text{A3})$$

Note that although there are accurate fully relativistic expressions for the electron and positron number densities in a strong magnetic field (see details in Mushtukov et al. 2019), we use here the approximation presented by Kaminker & Yakovlev (1993), where the basic assumption is that the electron positron pairs are in thermodynamic equilibrium at the high temperatures. It means also that we consider a non-degenerate plasma and use non-relativistic approximations. This is the situation we look at, so use of the simplified expressions is justified. The product of positron and electron number densities in thermodynamic equilibrium at zero magnetic field strength can be found as

$$n_{e+}^0 n_{e-}^0 = \frac{1}{2\pi^3 \lambda_C^6} e^{-2/t_r} t_r^3, \quad \lambda_C = \frac{\hbar}{m_e c}, \quad (\text{A4})$$

(Zeldovich & Novikov 1971). It is well known that the pair number density increases at high magnetic fields when $E_{\text{cyc}} \geq m_e c^2$, or $B \geq B_{\text{cr}} = m_e^2 c^3 / \hbar e \approx 4.414 \times 10^{13}$ G (see, e.g. Mushtukov et al. 2019). Here we take into account this kind of amplification using non-relativistic approximation

$$n_{e+}^B n_{e-} \approx n_{e+}^0 n_{e-}^0 \Delta b^2 (1 + 0.306 t_r) \coth^2 \left(\frac{\Delta b}{1 + 2.6 t_r} \right) \quad (\text{A5})$$

where

$$\Delta b = \frac{E_{\text{cyc}}}{2 k_B T} = \frac{\hbar e B}{m_e c} \cdot \frac{1}{2 k_B T}, \quad (\text{A6})$$

and the relative temperature t_r is

$$t_r = \frac{k_B T}{m_e c^2}. \quad (\text{A7})$$

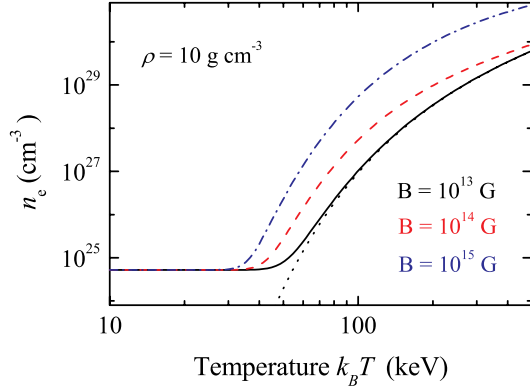


Figure A1. The total electron number density ($n_{e-} + n_{e+}$) vs. temperature for three magnetic field strengths: 10^{13} G (black solid curve), 10^{14} G (red dashed curve), and 10^{15} G (blue dot-dashed curve). The plasma density is fixed, 10 g cm^{-3} . The thermodynamic equilibrium positron number density at zero field strength (see Eq. A4) is shown with the black dotted curve.

Finally, using Eqs. (A1) and (A5) we obtain

$$n_{e+}^B = \frac{1}{2} \left(\sqrt{(\bar{Z} n_{\text{ion}})^2 + 4n_{e+}^B n_{e-}} - \bar{Z} n_{\text{ion}} \right). \quad (\text{A8})$$

In fact, the plasma density changes due to pair contribution

$$\rho' = \rho + m_e (n_{e+}^B + n_{e-}). \quad (\text{A9})$$

But we consider the plasma density determined using the ion number density only (Eq. A2) as a part of the input parameter in our computations, and, therefore, use it in opacity computations as well. It means that only the plasma density determined by Eq. (A2) has to be used for the Rosseland optical depth computations

$$d\tau = \rho \kappa(\rho, T, B) dx. \quad (\text{A10})$$

We note also, that the opacity calculations presented below can be easily recomputed from dimension $\text{cm}^2 \text{ g}^{-1}$ used here to dimension cm^{-1} by simple multiplication of opacity values presented here by corresponding grid point density.

An example of number density calculations using the approximations described below is presented in Fig. A1. Here we approximately reproduce the bottom panel of the Fig. (2) in Mushtukov et al. (2019) where more accurate relativistic expressions are used, and as can be seen from the figure, both results are in a good agreement for $k_B T < 200 \text{ keV}$.

The assumptions adopted in the paper are only appropriate for a non-degenerate plasma. This implies plasma temperatures need to be larger than the Fermi temperature, $T > T_F$. The Fermi temperature is determined by the plasma density and its value is significantly different for a non-quantizing magnetic field, at $k_B T < E_{\text{cyc}}$ and a strongly quantizing magnetic field in the opposite case.

The expression for the Fermi temperature in low field limit is

$$k_B T_{e-}^F = m_e c^2 (\gamma_r - 1), \quad (\text{A11})$$

where the parameters γ_r and x_r are determined as

$$\gamma_r = \sqrt{1 + x_r^2}, \quad x_r = \lambda_C (3\pi^2 n_{e-})^{1/3}. \quad (\text{A12})$$

In the opposite case, when $k_B T < E_{\text{cyc}}$ we consider the strongly-quantizing approximation, assuming that only the ground Landau level is occupied (Haensel et al. 2007). The Fermi temperature is significantly reduced at these conditions

$$k_B T_{e-}^F(B) = m_e c^2 (\gamma_B - 1), \quad (\text{A13})$$

where

$$\gamma_B = \sqrt{1 + x_B^2}, \quad x_B = \frac{2B_{\text{cr}}}{3B} x_r^3. \quad (\text{A14})$$

APPENDIX B: SPECIFIC OPACITIES

B1 Continuum opacity

The continuum opacity, for both electron scattering and free-free absorption are computed using the method described by Lai & Ho (2003); van Adelsberg & Lai (2006), see also Suleimanov et al. (2009). In the all cited papers the opacities were computed in cold plasma approximation for chemically pure (hydrogen or helium) atmospheres. We modified the method for the H/He mix and assume that the cold plasma approximation provides correct opacities at $E < E_{\text{cyc}}$. We note that the used opacities correctly transform to the non-magnetic opacities at $E \gg E_{\text{cyc}}$. The cyclotron opacity dominates at $E \sim E_{\text{cyc}}$, and the cold plasma approximation is not used for computations of the cyclotron opacity.

Vacuum polarization is also taken into account according to the description in van Adelsberg & Lai (2006). It is known that the plasma polarizability is dominating in the dielectric tensor at photon energies below some boundary energy $E_V = E_{\text{cyc}} V^{-1/2}$, where

$$V = \frac{3 \times 10^{28} \text{ cm}^{-3}}{n_e} \left(\frac{B}{B_{\text{cr}}} \right)^4, \quad (\text{B1})$$

and finally

$$E_V \approx (1.7 \times 10^4 n_e)^{1/2} B^{-1} \approx 413 \left(\frac{n_e}{10^{25}} \right)^{1/2} B_{12}^{-1} \text{ keV}. \quad (\text{B2})$$

In the opposite case, $E > E_V$, vacuum polarizability is dominating. There is a so called vacuum resonance at the photon energy $E = E_V$. At this condition the normal modes are mixed and the opacities in the both modes become equal.

Let us present the formulae for the continuum opacities. The scattering opacity from the mode i and the direction μ to the mode j and the direction μ' is

$$\kappa_{\text{es}}^{ij}(\mu, \mu') = \frac{3}{4} \frac{\sigma_T}{\rho} \sum_{\alpha=-1}^{+1} B_{\alpha} a_{\alpha}(i, \mu) a_{\alpha}(j, \mu'), \quad (\text{B3})$$

and the total scattering opacity from the mode j and the direction μ is

$$\kappa_{\text{es}}^j(\mu) = \frac{\sigma_T}{\rho} \sum_{\alpha=-1}^{+1} B_{\alpha} a_{\alpha}(j, \mu) \left(\sum_{i=1}^2 A_{\alpha}(i) \right), \quad (\text{B4})$$

where

$$B_{\alpha} = n_e t_e(\alpha) + \left(\frac{m_e}{m_p} \right)^2 n_i (A_{\text{H}} t_{\text{H}}(\alpha) + A_{\text{He}} t_{\text{He}}(\alpha)). \quad (\text{B5})$$

In the described approach the unit mode electric vector in the frame with the z-axis directed along magnetic field can be

presented as $\mathbf{E} = \mathbf{e}^j = e_0(iK_j, 1, iK_{z,j})$. The vector components are expressed using the ratio of the polarization ellipse $iK_j = E_x/E_y$, its projection on the z-axis $iK_{z,j} = E_z/E_y$, and the normalization $e_0 = (1 + K_j^2 + K_{z,j}^2)^{-1/2}$. The opacities are computed in the cyclic frame, and the corresponding squares of the cyclic vector components are

$$\begin{aligned} a_{\pm 1}(j, \mu) &= \left| \frac{1}{\sqrt{2}}(e_x^j + ie_y^j) \right|^2 \\ &= \frac{1 \pm (K_j \sin \theta + K_{z,j} \cos \theta)^2}{2(1 + K_j^2 + K_{z,j}^2)}, \end{aligned} \quad (\text{B6})$$

$$a_0(j, \mu) = \frac{(K_j \sin \theta - K_{z,j} \cos \theta)^2}{1 + K_j^2 + K_{z,j}^2}, \quad (\text{B7})$$

and

$$A_\alpha(j) = \frac{3}{2} \int_0^1 a_\alpha(j, \mu) d\mu. \quad (\text{B8})$$

They are computed using the ratio of the polarization ellipse axes

$$K_j = q \left(1 + (-1)^j \left(1 + \frac{r}{q^2} \right)^{1/2} \right), \quad (\text{B9})$$

where the polarization parameter q

$$q = -\frac{(\varepsilon^2 - g^2 - \varepsilon\eta) \sin^2 \theta + \varepsilon\eta(1 - r)}{2g\eta \cos \theta}, \quad (\text{B10})$$

and projection of the electric field vector on z-axis

$$K_{z,j} = -\frac{(\varepsilon - \eta) \sin \theta \cos \theta K_j + g \sin \theta}{\varepsilon \sin^2 \theta + \eta \cos^2 \theta}, \quad (\text{B11})$$

are computed using the components of the dielectric tensor ε , g , and η . We generalize their values, presented by [Lai & Ho \(2003\)](#) after [Ginzburg \(1970\)](#), for two ions, and present their shortened expressions without damping terms:

$$\varepsilon \pm g = 1 - \frac{v_e + v_i}{(1 \mp u_e^{1/2})(1 \pm u_H^{1/2})(1 \pm u_{\text{He}}^{1/2})}, \quad (\text{B12})$$

and

$$\eta = 1 - v_e - v_i. \quad (\text{B13})$$

Here we use the dimensionless values

$$v_e = \frac{E_p^2}{E^2}; \quad v_i = \frac{E_{p,i}^2}{E^2}, \quad (\text{B14})$$

and

$$u_e = \frac{E_{\text{cyc}}^2}{E^2}; \quad u_H = \frac{E_{\text{cyc,H}}^2}{E^2}; \quad u_{\text{He}} = \frac{E_{\text{cyc,He}}^2}{E^2}. \quad (\text{B15})$$

The positron contribution was taken into account at the plasma photon energy E_p computations by replacing $n_e \equiv n_{e-} + n_{e+}^B$ as it was declared in Sect. 2. The energy corresponding to plasma frequency, E_p , and the electron cyclotron energy E_{cyc} are also defined in Sect. 2. The energy $E_{p,i}$ corresponds to the ion plasma frequency $\nu_{p,i}^2 = Z^2 e^2 n_i / \pi A m_i$. The specific contribution of the protons and α -particles to the $\nu_{p,i}$ is equal, as $Z^2/A \approx 1$ for both ions. We use the total ion number density $n_i = n_H + n_{\text{He}}$. The common expression for the ion cyclotron energies is

$$E_{\text{cyc,(H,He)}} = \hbar \frac{ZeB}{Am_p c} \approx 6.35 \cdot 10^{-3} B_{12} \frac{Z}{A} \text{ keV}. \quad (\text{B16})$$

The vacuum polarization changes the dielectric tensor components and they have to be replaced as ([Potekhin et al. 2004](#))

$$\begin{aligned} \varepsilon &\rightarrow \varepsilon + a' \\ \eta &\rightarrow \eta + a' + q'. \end{aligned} \quad (\text{B17})$$

The value r is determined as

$$r = 1 + \frac{m'}{1 + a'} \sin^2 \theta. \quad (\text{B18})$$

Here m' , a' and q' are small corrections expressed as

$$\begin{aligned} m' &= -\frac{\alpha_f}{3\pi} \frac{b_Q^2}{3.75 + 2.7b_Q^{5/4} + b_Q^2} \\ a' &= -\frac{2\alpha_f}{9\pi} \ln \left(1 + \frac{b_Q^2}{5} \frac{1 + 0.25487b_Q^{3/4}}{1 + 0.75b_Q^{5/4}} \right) \\ q' &= \frac{7\alpha_f b_Q^2}{45\pi} \frac{1 + 1.2b_Q}{1 + 1.33b_Q + 0.56b_Q^2}, \end{aligned} \quad (\text{B19})$$

where $b_Q = B/B_{\text{cr}}$, and $\alpha_f = e^2/\hbar c \approx 1/137$.

The magnetic bremsstrahlung opacity in the mode j and the angle μ separately for collisions of electrons with protons and α -particles is

$$\kappa_{\text{H,He}}^j(\mu) = \sum_{\alpha=-1}^{+1} \zeta_{\text{H,He}}^j(\alpha) t_{\text{e,(H,He)}}(\alpha) a_\alpha(j, \mu), \quad (\text{B20})$$

where

$$\zeta_{\text{H,He}}^j(\pm 1) = \zeta_{\text{H,He}}^0 \Lambda_\perp, \quad \zeta_{\text{H,He}}^j(0) = \zeta_{\text{H,He}}^0 \Lambda_\parallel. \quad (\text{B21})$$

Here Λ_\perp and Λ_\parallel are the magnetic Gaunt factors ([Pavlov & Panov 1976](#); [Suleimanov et al. 2010](#); [Potekhin 2010](#)), and ζ_0 is the nonmagnetic bremsstrahlung opacity without Gaunt factor

$$\zeta_{\text{H,He}}^0 = \frac{2^{5/2} \pi^{3/2} \hbar^2 e^6}{c m_e^{3/2} (kT)^{1/2}} \frac{Z^2 A_{\text{H,He}} n_i n_e}{E^3 \rho} \left(1 - e^{-\frac{E}{kT}} \right). \quad (\text{B22})$$

We also use the following definitions

$$t_e(\pm 1) = \frac{1}{(1 \pm u_e^{1/2})^2 + (\gamma_{\text{e,H}}^\perp + \gamma_{\text{e,He}}^\perp + \gamma_{re})^2}, \quad (\text{B23})$$

$$t_{\text{H,He}}(\pm 1) = \frac{1}{(1 \mp u_{\text{H,He}}^{1/2})^2 + (\gamma_{\text{e,(H,He)}}^\perp + \gamma_{ri})^2}, \quad (\text{B24})$$

$$t_{\text{e,(H,He)}}(\pm 1) = \frac{1}{(1 \pm u_e^{1/2})^2 (1 \mp u_{\text{H,He}}^{1/2})^2 + \Gamma_{\text{e,(H,He)}}}, \quad (\text{B25})$$

and

$$t_e(0) = t_{\text{H,He}}(0) = t_{\text{e,(H,He)}}(0) = 1. \quad (\text{B26})$$

Here

$$\Gamma_{\text{e,(H,He)}} = \left(\gamma_{\text{e,(H,He)}}^\perp + (1 \pm u_e^{1/2}) \gamma_{ri} + (1 \mp u_{\text{H,He}}^{1/2}) \gamma_{re} \right)^2. \quad (\text{B27})$$

In the previous equations we used the effective radiative dimensionless dumping rates

$$\gamma_{re} = \frac{2e^2}{3m_e c^3 \hbar} E, \quad \gamma_{ri} = \frac{2Z^2 e^2}{3A m_p c^3 \hbar} E. \quad (\text{B28})$$

We note, that the rates for protons and α -particles are equal to each other, and we do not distinguish them. The relative

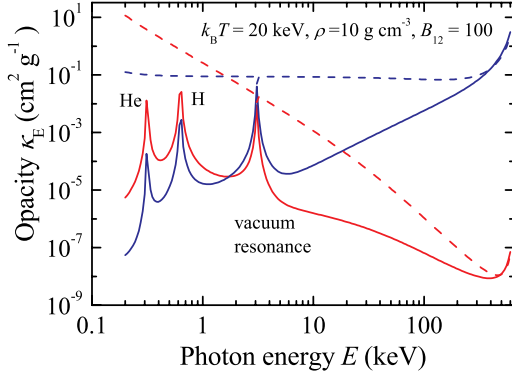


Figure B1. Dependence of the opacities due to free-free absorption (red curves) and electron scattering opacities (blue curves) on the photon energy for a plasma with the parameters presented in the plot. The magnetic field strength is 10^{14} G. Opacities in X-mode are shown by the solid curves, and the opacities in O-mode are shown by the dashed curves. Positions of the ion resonances for protons and α -particles as well as the position of the vacuum resonance are also shown.

effective dimensionless electron-ion collision rate across the magnetic field is

$$\gamma_{e,(H,He)}^{\perp} = \frac{\sqrt{2\pi}\hbar Z^2 e^4}{(m_e kT)^{1/2}} \frac{A_{H,He} n_i}{E^2} \left(1 - e^{-\frac{E}{kT}}\right) \Lambda_{\perp}. \quad (B29)$$

Examples of continuum opacities for some plasma parameters are shown in Fig. B1. We ignore here bremsstrahlung opacities due to e^-e^- , e^+e^+ , and e^-e^+ which could be potentially important at high magnetic fields and temperatures. We believe that the Rosseland mean opacity is dominated by photon scattering by electrons and positrons.

The electron scattering opacity can be smaller than Thomson scattering due to the Klein-Nishina reduction. It could be significant at high plasma temperatures. Therefore, we multiply the electron scattering opacity by the known ratio σ_{KN}/σ_T at every photon energy. Here $\sigma_T = 6.65 \times 10^{-25}$ cm² is the Thomson scattering cross-section. We perform this kind of reduction for the cyclotron opacity as well. The importance of this reduction for the Rosseland opacity of a weakly magnetized plasma is even more significant if Compton scattering is taken into account, see e.g. Paczynski (1983); Suleimanov et al. (2012a); Poutanen (2017), but we ignore it here.

B2 Cyclotron opacity

The opacities in the cyclotron line and the harmonics κ_j (cm² g⁻¹) for polarization modes $j=1$ (X-mode) and $j=2$ (O-mode) are computed using various approximate expressions.

For the normal mode opacities for the plasma domination case we use the approximate formulae derived by Pavlov et al. (1980a), (see also Suleimanov et al. 2012b). In particular, the X-mode opacity near the fundamental resonance is

$$\kappa_{11} \approx \frac{\sqrt{\pi}}{\hbar c \rho} \frac{E_p^2}{E} \frac{1 + \mu^2}{2\beta_T |\mu|} \exp(-x_1^2). \quad (B30)$$

The expressions for the O-mode opacity near the fundamental

resonance as well as the opacities at the harmonics can be found in Suleimanov et al. (2012b).

In comparison with the original version we have introduced some relativistic corrections by hands. So we use another definition for x_1 and corresponding values for higher harmonics

$$x_s = \frac{E - E_s}{\Delta E_{D,s}} \quad (B31)$$

by including the correct relativistic expression for the resonance and harmonic energies E_s instead of using the approximate linear shift relative to sE_{cyc}

$$E_s = \frac{m_e c^2}{1 - \mu^2} \left(\sqrt{1 + 2sB(1 - \mu^2)/B_{cr}} - 1 \right). \quad (B32)$$

Here s is the harmonic number, and $s=1$ for the fundamental resonance. The expression (B32) is correct for $\mu \neq 1$ only. There is only fundamental resonance at the energy E_{cyc} at $\mu = 1$.

The Doppler width of the harmonic $\Delta E_{D,s}$ is also corrected,

$$\Delta E_{D,s} = \min(E, E_s) \beta_T \mu \left(\frac{\sqrt{1 - \beta_T^2}}{1 - \mu \beta_T} \right). \quad (B33)$$

Here β_T is the ratio of the most probable thermal electron velocity to the speed of light. It is also corrected for relativistic effects,

$$\beta_T = \frac{v_T}{c} = \sqrt{2t_r} \left(\sqrt{1 + t_r^2} - t_r \right)^{1/2}, \quad (B34)$$

where t_r is defined by Eq. (A7). This expression provides the requirement $\beta_T < 1$ for any temperature, and can be derived from the condition $\partial f(p)/\partial p = 0$, where $f(p) \sim p^2 \exp(-\sqrt{1 + p^2}/t_r)$ is the probability distribution of electron momenta in accordance with the relativistic Maxwell-Jüttner distribution, and $p = |\mathbf{v}|/c\sqrt{1 - v^2/c^2}$ is the module of the dimensionless relativistic momentum.

In expression (B30) as well as in all the following expressions for the cyclotron opacities, the Gaussian broadening function is used instead of integration over the electron momenta. It is acceptable for $t_r \ll 1$, but for the high temperature cases the resonance condition is not fulfilled for the high energy electrons with the momenta directed to the observer. Therefore, we cut the cyclotron opacity at energies higher than the cutoff energy

$$E_{cut,s} = \frac{m_e c^2}{\sqrt{1 - \mu^2}} \left(\sqrt{1 + 2sB/B_{cr}} - 1 \right) \quad (B35)$$

which is determined separately for the fundamental resonance and every harmonic, see, e.g. Schwarm et al. (2017).

For the case of the vacuum domination we also use the approximations for the opacities near the fundamental resonance from Pavlov et al. (1980a). The opacity at the fundamental resonance in X-mode is

$$\kappa_{11} \approx \frac{\sqrt{\pi}}{\hbar c \rho} \frac{E_p^2}{E} \frac{1}{2\beta_T |\mu|} \exp(-x_1^2). \quad (B36)$$

This expression is correct, if the value $V\beta_T\mu(1 - \mu^2) > 1$ (see detail in Pavlov et al. 1980a). In the opposite case we use Eq. (B30). The same condition we use for separation of the expressions describing the opacities near the fundamental resonance in O-mode.

The opacities near the harmonics in X-mode for the case of the vacuum dominance are taken from [Melrose & Zhelezniakov \(1981\)](#)

$$\kappa_{s1} \approx \frac{\sqrt{\pi}}{\hbar c \rho} \frac{E_p^2}{E} \frac{1}{\beta_T |\mu|} \frac{\kappa_V}{(s-1)!} \exp(-x_s^2), \quad (\text{B37})$$

where

$$\kappa_V = \frac{\sinh(E/2k_B T)}{(\exp(E_1/k_B T) - 1)^s} \left(\frac{\varepsilon E(1 - \mu^2)}{2E_1} \right)^{s-1}. \quad (\text{B38})$$

Here $\varepsilon = E/m_e c^2$ is the relative photon energy. These expressions are correct for the case $k_B T \sim E_{\text{cyc}}$. The cyclotron opacity is important for the Rosseland opacity computation in this case only.

All the opacities near the fundamental resonance and the harmonics in O-mode for the case of the vacuum domination are computed using the expressions for the opacities in X-mode

$$\kappa_{s2} \approx \kappa_{s1} \left(\mu^2 + \frac{E_1}{4k_B T} \beta_T^2 \right), \quad (\text{B39})$$

but the separation condition for the harmonics is the same as for continuum opacities, i.e. we use Eq. (B39) if $E > E_V$. In fact the transition of the cyclotron opacity across the vacuum resonance is much more complicated (see, e.g. [Pavlov et al. 1980a](#)) and we did not consider it here in detail.

Examples of cyclotron opacities are presented in Fig. B2. It reproduces Figs. 5a and 6a published by [Mushtukov et al. \(2016\)](#). It is clear that our simplified approach reproduces well the resonance and harmonic energies, although the line widths are slightly underestimated (especially for $\mu \rightarrow 0$) because we ignore the natural Landau level width, and the opacities in the harmonics are overestimated. The cyclotron opacities are presented together with the continuum electron scattering opacities at low energies.

All the expressions presented above are not sufficiently correct at high temperatures and using of them leads to cyclotron opacity overestimation. This is the reason why we do not use them for the cyclotron harmonic opacities at temperatures above 45 keV and the large angles provide too broad harmonics for the plasma domination case. At these conditions we use the opacities derived from the fitting formulae for the high-temperature cyclotron-synchrotron emissivities obtained by [Pandya et al. \(2016\)](#):

$$\kappa_{\text{syn}}^j = \frac{k_{\text{syn}}}{\rho} (X \pm Y), \quad (\text{B40})$$

where the sign “+” corresponds to X-mode, and the sign “−” corresponds to O-mode. Here

$$k_{\text{syn}} = \frac{\sqrt{2}\pi}{27} e^2 n_e \sqrt{1 - \mu^2} E_{\text{cyc}} \exp(-\epsilon^{1/3}) B_E^{-1}, \quad (\text{B41})$$

$$X = (\epsilon^{1/2} + 2^{11/12} \epsilon^{1/6})^2, \quad (\text{B42})$$

and

$$Y = (\epsilon^{1/2} + a_t 2^{11/12} \epsilon^{1/6})^2, \quad (\text{B43})$$

where

$$a_t = \frac{7t_r^{24/25} + 35}{10t_r^{24/25} + 75}. \quad (\text{B44})$$

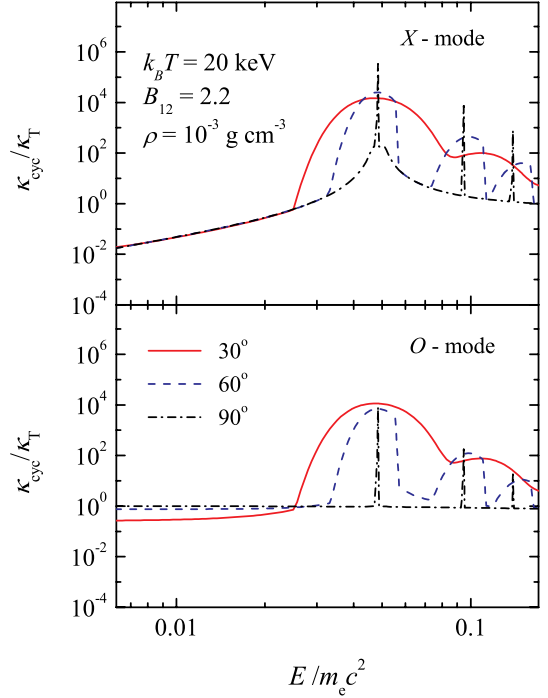


Figure B2. Dependence of the cyclotron plus continuum electron scattering opacities on the relative photon energy for a plasma with temperature $k_B T = 20$ keV, $\rho = 10^{-3} \text{ g cm}^{-3}$, and $B = 2.2 \times 10^{12} \text{ G}$. All the opacities are computed for the vacuum domination case.

The dimensionless relative energy $\epsilon = E/E_c$ is the photon energy normalized by the energy

$$E_c = \frac{2}{9} E_{\text{cyc}} t_r^2 \sqrt{1 - \mu^2}, \quad (\text{B45})$$

and B_E is the Planck function. The opacity determined by Eq. (B40) is used as the cyclotron opacity of the harmonic if $k_B T > 45$ keV and the plasma domination case. The opacities near the fundamental resonance and all the opacities for the case of the vacuum dominance are computed using Eqs. (B30), (B36), (B37), and (B39) for any plasma temperature.

B3 Two-photon pair production

Interaction of two photons with energies E and E' can create an electron-positron pair, if their common relative energy in the centre-of-momentum frame exceeds the pair mass, $\varepsilon \varepsilon' (1 - \mu') > 2$, where μ' is the cosine of the angle between the directions of the photon propagations, and $\varepsilon = E/m_e c^2$ is the relative photon energy. The corresponding opacity is described in detail by [Beloborodov \(1999\)](#). We simplified his expressions as we considered pair creation by the almost isotropic blackbody radiation. As a result the opacity is

$$\kappa_{\gamma\gamma}(E) = \frac{2\pi}{c\rho} \int_0^\infty \frac{B_{E'} dE'}{E'} \int_{-1}^{+1} (1 - \mu') \sigma_{\gamma\gamma}(\varepsilon_c) d\mu'. \quad (\text{B46})$$

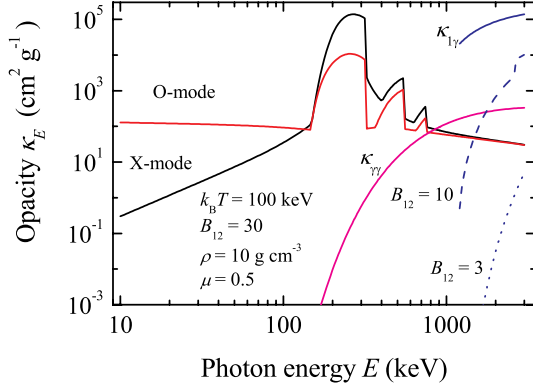


Figure B3. Dependence of the cyclotron plus continuum electron scattering opacities on the relative photon energy for a plasma with temperature $k_B T = 20$ keV, $\rho = 10^{-3}$ g cm $^{-3}$, and $B = 2.2 \times 10^{12}$ G. All the opacities are computed for the vacuum domination case.

Here $\sigma_{\gamma\gamma}(\varepsilon_c)$ is the cross-section of the two-photon interaction

$$\sigma_{\gamma\gamma}(\varepsilon_c) = \frac{3\sigma_T}{8\varepsilon_c^2} \left(2 + \frac{2}{\varepsilon_c^2} + \frac{1}{\varepsilon_c^4} \right) \ln \left(\varepsilon_c + \sqrt{\varepsilon_c^2 - 1} \right) - \frac{3\sigma_T}{8\varepsilon_c^2} \left(1 + \frac{1}{\varepsilon_c^2} \right) \sqrt{1 - \frac{1}{\varepsilon_c^2}}, \quad (\text{B47})$$

depending on the relative photon energy in the centre-of-momentum z_c

$$\varepsilon_c = (\varepsilon'/\varepsilon_{\text{thr}})^{1/2}, \quad (\text{B48})$$

where

$$\varepsilon_{\text{thr}} = \frac{2}{\varepsilon(1 - \mu')}. \quad (\text{B49})$$

The cross-section $\sigma_{\gamma\gamma}(\varepsilon_c)$ equals zero if $\varepsilon' < \varepsilon_{\text{thr}}$.

B4 One-photon pair production in a strong magnetic field

In a strong magnetic field a single photon with energy $\varepsilon_{\perp} \equiv \varepsilon\sqrt{1 - \mu^2} > 2$ can transform to an electron-positron pair. We consider here this process as an additional opacity, and use two approximate expressions for the attenuation rate. The first one was presented by [Daugherty & Harding \(1983\)](#) and we use it for the strong enough magnetic field $B > 0.5B_{\text{cr}}$. If the photon energy is larger than the $\varepsilon_{\perp} > 2$, then

$$\kappa_{1\gamma}(\mu, E) \approx 0.23 \frac{\alpha_f}{\lambda_C} \frac{B\sqrt{1 - \mu^2}}{B_{\text{cr}}} \exp \left[-\frac{4f(E, B)}{3\chi} \right] \frac{1}{\rho}. \quad (\text{B50})$$

In the opposite case, $\varepsilon_{\perp} < 2$, the considered opacity equals zero, $\kappa_{1\gamma} = 0$. Here the variable χ is determined as

$$\chi = \frac{\varepsilon_{\perp}}{2} \frac{B}{B_{\text{cr}}}, \quad (\text{B51})$$

the fitting function is

$$f(E, B) \approx 1 + 0.42 \left(\frac{\varepsilon_{\perp}}{2} \right)^{-2.7} \left(\frac{B}{B_{\text{cr}}} \right)^{-0.0038}, \quad (\text{B52})$$

and $\alpha_f \approx 1/137$ is the fine-structure constant. The presented one-photon annihilation opacity is averaged over the photon

polarizations and over the photon energy, smearing the numerous saw-edges existing in the accurate attenuation rate.

At relatively low magnetic fields Eq. (B50) significantly overestimates the correct pair creation rate. For this case another approximation, suggested by [Baring \(1991\)](#), is used:

$$\kappa_{1\gamma}(\mu, E) \approx \frac{\alpha_f}{\lambda_C} \frac{B\sqrt{1 - \mu^2}}{\varepsilon_{\perp}^2 B_{\text{cr}}} \Lambda(\varepsilon_{\perp}) \exp \left[-\frac{\phi B_{\text{cr}}}{4B} \right] \frac{1}{\rho}. \quad (\text{B53})$$

Here

$$\Lambda(\varepsilon_{\perp}) = \frac{3\varepsilon_{\perp}^2 - 4}{(\varepsilon_{\perp} + 2)^2} \sqrt{\frac{\varepsilon_{\perp}^2 - 4}{\zeta\phi}}, \quad (\text{B54})$$

$$\phi = 4\varepsilon_{\perp} - \zeta(\varepsilon_{\perp}^2 - 4), \quad (\text{B55})$$

and

$$\zeta = \log \left(\frac{\varepsilon_{\perp} + 2}{\varepsilon_{\perp} - 2} \right). \quad (\text{B56})$$

Examples of the $\kappa_{1\gamma}(\mu, E)$ dependence on photon energy for three different magnetic field strengths are shown in Fig. B3.

APPENDIX C: DATA FILES AND THE INTERPOLATION CODE

The arXiv ‘‘Source Files’’ contain the files with the grid Rosseland opacities across and along magnetic field lines. The opacity database is also available via https://github.com/alexandermushtukov/RT_mag_opacity. The opacities represented in different files are computed under different assumptions about contribution of electron-positron pair. In particular, the files contained in archives `ross1.zip` and `ross2.zip` correspond to the opacities across and along the field respectively with the pairs in thermodynamic equilibrium and opacities due to pair creation taken into account. The files contained in archives `ross3.zip` and `ross4.zip` correspond to the opacities across and along the field respectively with no pairs, but the opacities due to pair creation taken into account. The files contained in archives `ross5.zip` and `ross6.zip` correspond to the opacities across and along the field respectively computed without pairs participation at all.

Every archive file contains information about the Rosseland opacities calculated for 14 values of magnetic fields $\lg B = 10.5, 11.0, 11.5, 11.75, 12.0, 12.25, 12.5, 12.75, 13.0, 13.25, 13.5, 14.0, 14.5, 15.0$, where B is measured in Gauss, for 19 values of mass density, from $\lg \rho = -6$ to 3 with the step 0.5, and for 85 values of temperature, from $\lg T = 0$ to 2.52 with the step 0.03.

Every archive file is organised as a set of 14 two-dimensional tables of the opacities collected in separate data files named like `ross1_b1175.dat`. Every two-dimensional table is computed for the magnetic field strength marked in the file name. In the example above, the magnetic field strength corresponds to $\lg B = 11.75$. Each table consists of 85 rows corresponding to the grid temperatures and 21 columns. In the first column, the temperature in units of keV is presented, in the second column, the values $\lg T$ are presented, and in the rest columns, the values of the Rosseland mean opacities for 19 values of the plasma density are presented, starting with $\lg \rho = -6$ (third column).

We also provide an interpolation code finding the Rosseland opacity for given values of B , T , and ρ inside of the grid, and a test code. Both codes are in file `ross.intSn.f`. Before use, all the data files have to be unpacked into the same directory with the code (or possibly in a separate directory, but in this case, the accurate ways to them have to be determined by `open()` operators).

The interpolation subroutine `abross1(istart,rho,ttt,bb,abrss)` has three input parameters `bb` $\equiv B(\text{G})$, `ttt` $\equiv k_{\text{B}}T(\text{keV})$, `rho` $\equiv \rho(\text{g cm}^{-3})$, one output parameter `abross` $\equiv \kappa_{\text{R}}$, and one key `istart`. Before interpolation, a choice of the type of the necessary Rosseland opacities has to be made, which is coded as `rossN`. For this aim, the subroutine `abross1` has to be called with the key `istart=N` and arbitrary values of other input parameters. Then the necessary interpolation can be performed by calling the subroutine with `istart=0` and the actual values of the input parameters. It is possible to make as many opacity interpolations as it is necessary after the establishment of some Rosseland opacity type. A new call of the subroutine with another `istart=N'` has to be performed if it is necessary to find another Rosseland opacity type, coded as `rossN'`.